Prediction of EMI Filter Attenuation in Power-Electronic Converters via Circuit Simulation

S. Negri, *Member, IEEE*, G. Spadacini, *Senior Member, IEEE*, F. Grassi, *Senior Member, IEEE*, and S. A. Pignari, *Fellow, IEEE*

***Abstract*—This paper investigates the conducted-emission (CE) suppression characteristics of electromagnetic-interference (EMI) filters used in power-electronic equipment by time-domain circuit simulation. An operational definition of insertion attenuation is introduced by comparing the CE in the absence and in the presence of the EMI filter. For the sake of exemplification, the analysis focuses on switched-mode dc/dc converters. It is shown that the EMI-filter attenuation behaves differently from the standard insertion loss (IL) and exhibits peculiar properties in these circuits. Namely, its response is known at discrete frequencies where the converter generates CE and may strongly depend on the harmonic index so to jump between quite different levels from a harmonic component to the next one, with a pseudo-periodic behavior which can be related to the duty cycle. This effect is caused by circuit nonlinearity and is partially mitigated if the simulation accounts for two practically relevant aspects: random instability of the duty cycle and resolution bandwidth of the EMI receiver. The dependence of the common-mode (CM) and differential-mode attenuations on the loading conditions and duty cycle is analyzed, and it is shown that linear IL models provide reasonable predictions of CM attenuation only. Finally, experimental evidence of the unveiled phenomena is presented.**

***Index Terms*— Conducted emission (CE), electromagnetic interference (EMI), EMI filters, power electronics.**

I. Introduction

The ever increasing availability of powerful computer simulation resources is driving the industrial practice of early-time prototyping towards the use of virtual test beds so to avoid costly after-the-fact remedies. This general trend is well perceived in the field of Electromagnetic Compatibility, where computer solvers are largely used to predict electromagnetic interference (EMI) phenomena in complex systems. In this respect, several literature contributions have recently proposed circuit models to characterize power-electronic converters as EMI sources, and to predict the propagation of conducted emissions (CE) along power cables. Two different rationales can be recognized: a) linear behavioral modeling; b) component-level circuit modeling.

Behavioral models are black-box equivalent circuits identified from characterization measurements [1]-[4]. Namely, any power-electronic converter is treated as a linear, active, multi-terminal element [1] composed of current/voltage sources and immittances, whose frequency response is identified by suitable measurement procedures in controlled test setups, involving frequency-domain [2] or time-domain instrumentation [3]. The obtained models are valid above the fundamental switching frequency, inherently include parasitic effects (e.g., stray capacitances) and enable computationally efficient CE predictions by frequency-domain computer codes [4]. As a limitation, the low-frequency functional working point (e.g., the variable dc/ac power) cannot be modeled and associated with the predicted CE. Moreover, the underlying assumption of linearity is not to be taken for granted, even at the high frequencies of interest for EMI analysis, given the nonlinear nature of power-electronic circuits.

In a complementary approach, component-level circuit models are explicit representations of the internal converter components, including nonlinear valves (diodes, transistors), solved in the time domain by circuit-simulation software (e.g., SPICE) [5]-[7]. Time-domain waveforms are processed by the Fast Fourier Transform (FFT) to evaluate spectra according to CE standards [8]. Lumped parasitic capacitors and inductors must be included in the circuit representation and their determination requires ad-hoc component measurements or full-wave electromagnetic simulation [7], [9]. Eventually, the circuit model can be used to predict both the functional operation of converters and high-frequency EMI effects of interest for CE analysis [6].

Among different applications, the virtual assessment of an EMI filter or its customized prototyping for a specific system were paid much attention in the framework of linear behavioral-modeling techniques [2], [3]. Conversely, little attention has been paid so far to the inclusion and assessment of EMI filters in time-domain circuit simulation. In principle, this is made straightforward by the availability of modeling strategies for extracting EMI-filter parasitics and/or constructing SPICE-compatible models from frequency-domain measurements [10]-[14]. The equivalent circuit can be used in time-domain

Manuscript received Nov. 5, 2021; revised March 2, 2022; accepted April 2, 2022.

S. Negri, G. Spadacini, F. Grassi, and S. A. Pignari are with Politecnico di Milano, Dept. of Electronics, Information and Bioengineering, 20133, Milan, Italy (e-mail: {simone.negri, giordano.spadacini, flavia.grassi, sergio.pignari} @polimi.it).

Published version available, DOI 10.1109/TEMC.2022.3165377

simulations for predicting common-mode (CM) and differential-mode (DM) currents. However, to the authors' knowledge, the potential of time-domain circuit simulation was never explored to investigate the suppression characteristics of EMI filters, that is, the comparison between CE predicted in the absence and in the presence of the filter. This paper will put in evidence that subtle, nontrivial phenomena characterize predictions and must be properly addressed.

Specifically, Section II focuses on the comparison of CE predicted in the absence and the presence of an EMI filter, which allows for an operational definition of insertion attenuation in nonlinear switching circuits by extending the insertion loss (IL) concept defined in linear setups [15]. From Section III the focus is put on the case of switched-mode dc/dc converters (a step-down circuit topology is exemplified). It is shown that filter attenuation behaves quite differently from IL, since it jumps between different levels from a harmonic CE component to the next one with pseudo-periodic behavior. Results are reviewed in Section IV after modeling two practically relevant conditions, namely, random instability of the duty cycle and finite resolution bandwidth (RBW) of the EMI receiver. Though nonlinear phenomena are partially mitigated by such conditions, and filter attenuation tends to assume a well-defined IL-like frequency response, the added value of time-domain nonlinear circuit simulation will be still confirmed. Indeed, it can predict CM and DM insertion attenuation associated to the functional operation (duty cycle, loading) of the converter. Moreover, in Section V it will be explicitly shown that predictions obtained by linear IL models would lead to reasonable estimates of filter performances for the CM only. Experimental evidence of the phenomena discovered by simulations is presented in Section VI. Finally, Section VII draws concluding remarks.

II. Insertion Attenuation of Filters By Time-Domain Circuit Simulation

A. The Standard IL in Linear Circuits

To introduce the proposed methodology, it is useful recalling first the standard concept of IL defined in CISPR 17 [15]. According to Fig. 1, the EMI filter is connected to a linear, resistive source (V_S, R_S) and load (R_L) in two configurations, called "symmetrical" and "asymmetrical" setup, to excite a DM and CM response, respectively [15]. The assumption of linearity allows the definition of modal ILs in the frequency domain as

$$IL_{DM} = 20\log_{10}\left|\frac{V_{WO}}{V_{DM}}\right| \quad (1)$$

$$IL_{CM} = 20\log_{10}\left|\frac{V_{WO}}{V_{CM}}\right| \quad (2)$$

where V_{DM}, V_{CM} are voltages across the load R_L in Fig. 1, and $V_{WO}=V_S R_L/(R_S+R_L)$ would be the voltage across R_L if the source and load were directly connected without the filter. Therefore, modal ILs are figures of merit of the attenuation provided by the filter in specific conditions. They do not depend on the source V_S since, by linearity, both the denominator and numerator in (1)-(2) are proportional to V_S. Conversely, they depend on source and load resistances. Standardized CISPR-17 setups involve the specific cases: a) R_S=R_L=50 Ω; b) R_S=100 Ω, R_L=0.1 Ω; c) R_S=0.1 Ω, R_L=100 Ω [13].

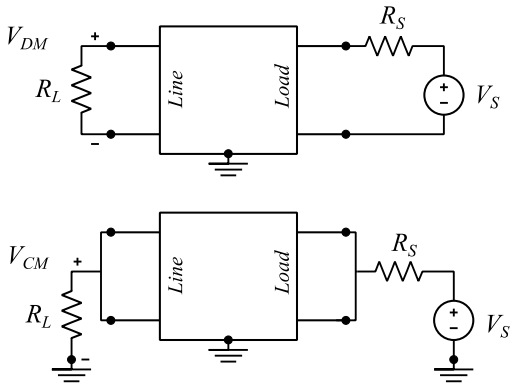

Fig. 1 – CISPR-17 test setups for measuring the IL of an EMI filter (central block). Top: Symmetrical mode (DM); Bottom: Asymmetrical mode (CM).

If a circuit model of the EMI filter is available, a circuit solver (e.g., SPICE) can be used to predict IL by simulating the measurement setups in Fig. 1. This circuit model could be an explicit representation of internal filter components (capacitors, resistors, CM chokes) accounting for their non-ideal behavior [10], or an equivalent circuit derived from external S-parameter measurement [12].

The frequency domain (phasor analysis) is the natural tool to perform such linear-circuit simulations, since it directly provides the frequency response of V_{DM}, V_{CM}. However, in view of the extension to nonlinear switching circuits, let us also consider the alternative time-domain procedure described in the following.

An arbitrary periodic waveform $v_S(t)$ with period T_0 (fundamental frequency f_0=1/T_0) is assigned to the source in Fig. 1, while load waveforms $v_{DM}(t)$, $v_{CM}(t)$ (in the symmetrical and asymmetrical setups, respectively), $v_{WO}(t)$ (in the setup without filter) are computed by time-domain circuit simulations. In post-processing, waveforms are transformed into spectra V_{DM}, V_{CM}, V_{WO} by FFT. Insertion attenuations $A_{X,n}$ (X=*DM, CM*) are evaluated in correspondence to the harmonic components of the Fourier series (i.e., where voltage-magnitude peaks are located) by

$$A_{X,n} = 20\log_{10}\left|\frac{V_{WO,n}}{V_{X,n}}\right| = 20\log_{10}\left|V_{WO,n}\right| - 20\log_{10}\left|V_{X,n}\right| \quad (3)$$

where n=1, 2, 3, … is the harmonic index. This process is represented in Fig. 2, which puts in evidence the meaning of attenuation A_n as the difference (in dB) between the voltage peaks without and with filter at the frequency nf_0. The computation is intentionally limited to harmonic frequencies since the spectrum of periodic signals is composed of narrowband peaks. If the operation (3) was extended to any

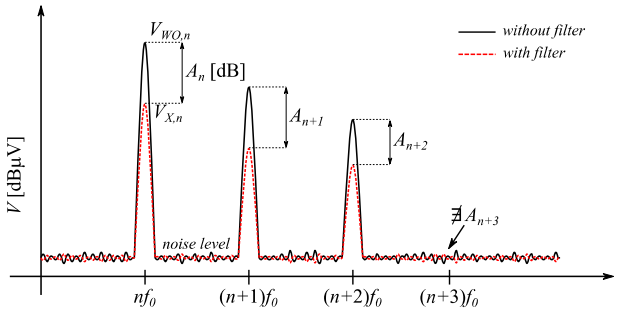

Fig. 2 Operational definition of insertion attenuation from CE spectra obtained by time-domain simulation and subsequent FFT.

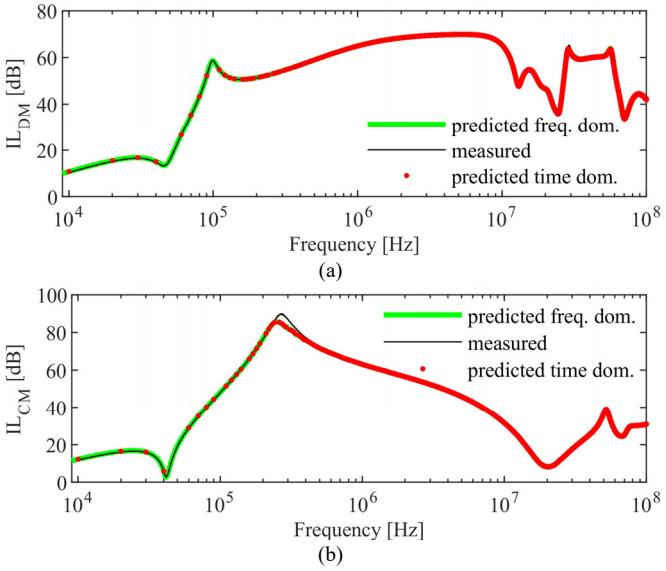

Fig. 3 – (a) DM IL and (b) CM IL of a specific filter used for exemplification throughout this paper. Solid lines represent the measured IL (black) and the IL predicted by frequency-domain circuit simulation (green). Red dots represent insertion attenuations (3) predicted by time-domain circuit simulation.

frequency between two harmonics, the result would be meaningless (that is, operationally determined by a numerical noise level). Similarly, $A_{X,n}$ shall not be computed in case of null harmonic components. The properties of linear time-invariant circuits guarantee that the attenuations (3) will be samples of the IL frequency response in (1)-(2), apart from numerical errors arising in the articulated computational process [16].

For the sake of exemplification, the black-box SPICE model of the EMI filter developed in [12] will be used together with the solver [17] in the remainder of this paper. The SPICE subcircuit netlist is available through IEEE DataPort [18]. Modal (50 Ω) ILs computed by SPICE simulations in the frequency domain and CISPR-17 measurements carried out by a vector network analyzer are plotted in Fig. 3. In these plots, single dots represent the harmonic attenuations (3) evaluated by time-domain SPICE simulations involving a square-wave source $v_S(t)$ with f_0=10 kHz, duty cycle δ=0.8, and 1 ps rise/fall times, whose harmonics are null for n=5, 10, 15, etc. As expected, harmonic attenuations are discrete samples of the IL (dots get closer and closer in a semilogarithmic scale, till they resemble a thick line). In passing, the good agreement with IL measurements supports the validity of the proposed filter circuit.

B. Insertion Attenuation in Nonlinear Circuits

For switching circuits generating periodic waveforms like power-electronic converters modeled at component level, no solution in the frequency domain is possible. Therefore, the time-domain procedure introduced above is the only viable solution to predict the insertion attenuation of EMI filters.

Fig. 4 shows the reference setups for the evaluation of CE with and without filter. The feeding line, the line-impedance stabilization network (LISN), the EMI filter, the converter and the load are represented by generic functional blocks, as their inner content depends on the specific applicative domain (e.g., ac/dc systems, CE standards, etc.). In this respect, the circuit refers to a two-wire system (e.g., dc or single-phase ac) without loss of generality.

Provided that circuit models are available for each block, offering a satisfactory description of both their functional operation and their high-frequency parasitic effects, setups in Fig. 4 can be easily inputted in a circuit solver to predicted CE in time domain, [5]-[7]. The obtained waveforms of LISN voltages $v_1(t)$, $v_2(t)$ are stored after a suitable time frame (so to allow the circuit to reach functional steady-state conditions), their spectra V_1, V_2 are evaluated by FFT, and finally transformed into CM/DM by

$$V_{\substack{CM\\DM}} = (V_1 \pm V_2)/2 \tag{4}$$

The obtained CM/DM spectra with and without EMI filter will be composed of narrowband peaks at the harmonics nf_0, n=1, 2, 3, … of the switching frequency f_0. Therefore, the insertion attenuation of the filter can be defined by (3) for each harmonic component.

III. Case Study

While the standard IL (1)-(2) is defined in a linear circuit, therefore conditions are univocally specified by two terminal resistors, such a generality does not hold for the insertion attenuation in power-electronic systems. For any EMI filter, results are strictly dependent on the specific configuration of the reference setups in Fig. 4, that is, on converter type and technology context. The remainder of this paper will focus on switched-mode dc/dc converters. A case study comprising a step-down (buck) converter for vehicle applications will be analyzed without claim of exhaustiveness. Nevertheless, general properties will emerge from the observed results.

A. System Under Analysis

The general setup in Fig. 4(a) is implemented in SPICE as shown in Fig. 5. The inner block U_1 contains the subcircuit of the EMI filter [12], [18]. On the right, elements C_1 and C_2 (input and output capacitors), M_1 (power MOSFET N1STWNM80 by STMicroelectronics), D_3 (diode RFN10NS8D by ROHM Semiconductor), L_1 and L_4 (output inductors) are components of the converter. Capacitors C_7, C_8, C_9 establish a parasitic path for CM currents to flow. Additional lumped parasitic

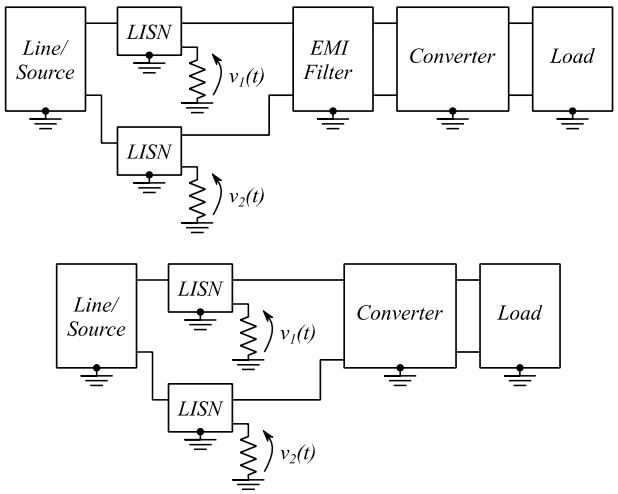

Fig. 4 – Reference circuits for the definition of insertion attenuation of EMI filters in power-electronics converters. Top: setup with filter; Bottom: setup without filter.

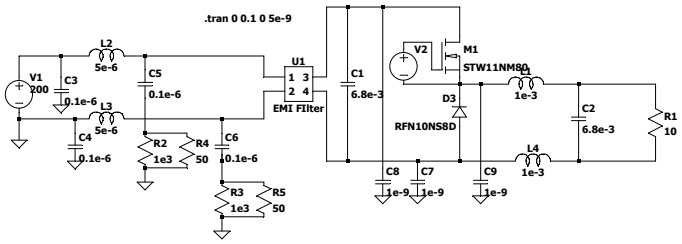

Fig. 5 – Reference circuit in Fig. 4 particularized for a step-down converter in a CISPR-25 test setup.

parameters (series inductance of capacitors, parallel capacitance of inductors) could be included in the circuit, which are dependent on the physical properties of specific equipment and components [6]-[7], [9]. Here, the circuit is intentionally kept essential to demonstrative purposes. On the left, there is a 200 Vdc voltage source V_1 and components of the standard circuit of two CISPR-25 LISNs [19]. The rightmost resistor R_1 represents the converter load, and the voltage source V_2 at the gate of M1 drives the valve by a pulse with f_0=10 kHz and constant duty-cycle δ. Load resistance and duty-cycle will be specified case by case in the following descriptions.

B. Attenuation Dependence on the Harmonic Index

For R_1 = 50 Ω, δ = 0.8 (load voltage 160 V, power 512 W), modal CE voltages (4) with and without the EMI filter, obtained from time-domain simulations, are plotted in Fig. 6 in the frequency range 9 kHz-100 MHz. One can visually appreciate the shape of the spectral envelope, as the large number of narrowband peaks (10^4 peaks at multiple frequencies nf_0) piles up in uniformly shaded areas. Similar plots are common in the literature, and used to infer properties, like the dominance of DM at low frequency, of CM at high frequency, and possible compliance with piecewise-linear CE limits [3], [5]-[7]. Seldom, attention has been paid to the behavior of single CE peaks, which are mostly indistinguishable in the plots. The CM/DM insertion attenuations, represented by dots in Fig. 7, unveil this behavior and highlight the operation of the EMI filter at different harmonics.

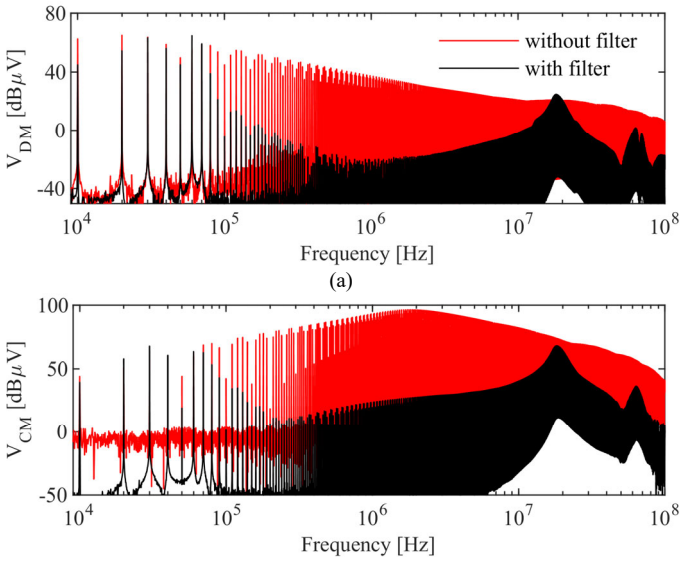

Fig. 6 – (a) DM and (b) CM CE of the step-down converter without EMI filter (red line) and with EMI filter (black line), for duty cycle δ=0.8, load R_1=50 Ω.

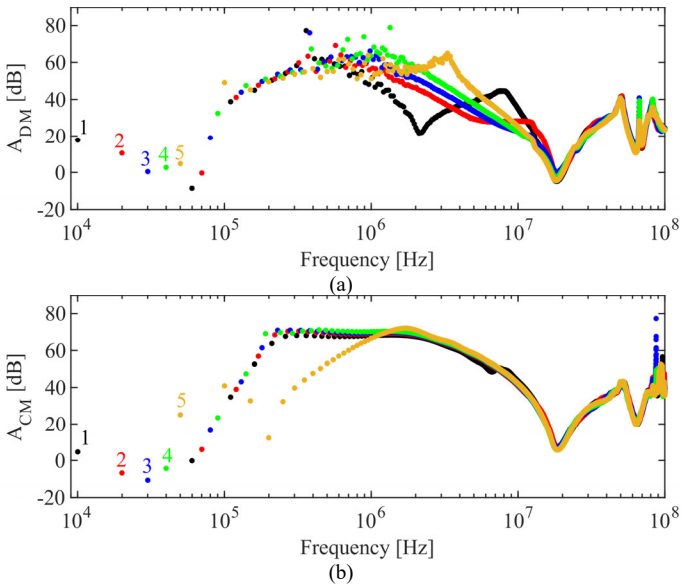

Fig. 7 – (a) DM and (b) CM insertion attenuation of the EMI filter in the step-down converter circuit, for duty cycle δ=0.8 and load R_1=50 Ω. One can appreciate up to five apparent lines (different colors) emerging from the accumulation of dots.

Unsurprisingly, attenuation may take negative values (i.e., filter insertion increases CE) as this commonly happens for the CISPR IL in case of non-50 Ω terminal resistors [15]. Conversely, a noticeable aspect is that the path of dots separates into up to five curves in Fig. 7, which are apparent lines created by the accumulation of dots, depending on the associated harmonic index (different colors are used to increase visibility). This phenomenon can be fully appreciated in Fig. 8, which represents a zoom of the DM CE spectra in Fig. 6(a) and the DM attenuation in Fig. 7(a). Peaks and their difference in dB recur with a pseudo-periodic pattern every five harmonic indexes, forming five levels of attenuations.

Although justifying complex numerical solutions is generally hard, it is straightforward to provide an analytical interpretation

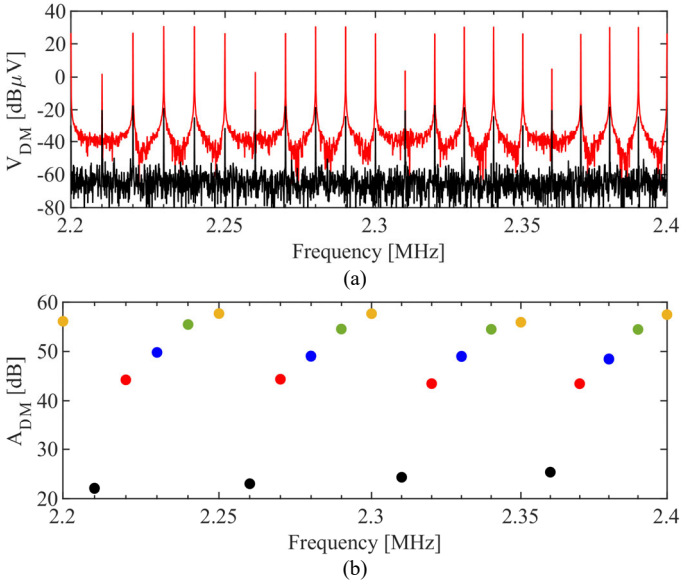

Fig. 8 – Zoom in a narrow frequency range of (a) the DM CE spectra in Fig. 6(a) and (b) the DM insertion attenuation in Fig. 7(a).

of the underlying phenomenon which supports confidence in results. Namely, the driving source V2 is a rectangular pulse with constant duty-cycle δ, therefore its complex Fourier spectrum is proportional to the term

$$1 - e^{-j2\pi n\delta} \tag{5}$$

which is periodic with the harmonic index n, and its period is determined by the smallest integer assumed by the product $n\delta$. For δ=0.8=4/5, the period is n=5. Hence, harmonics can be grouped in five sets, corresponding to n=5k+1, n=5k+2, n=5k+3, n=5k+4, n=5k+5, with k=0, 1, 2, etc.

The last set n=5k+5 is a noteworthy case to be discussed, since it makes the term (5) equal to zero, that is, the driving source has no harmonics for n=5, 10, 15, etc. If the circuit were linear and time-invariant, by virtue of the superposition theorem [16], this set of missing harmonics of the source would be unexcited, that is, missing, in any other voltage and current (an example was already provided in Sec. II.A while discussing the conventional IL, see Fig. 3). Conversely, this set does exist in the system under analysis, as shown in Fig. 7-8. Indeed, in a nonlinear circuit with periodic sources and solutions, each harmonic component in a voltage/current receives mutual contributions from all the harmonics of the source [16].

In general, the complex interaction of harmonics in the nonlinear circuit leads to a different behavior of filter attenuation depending on the five characteristic sets of indexes defined by different colors in Fig. 7 and 8. Some curves may get close enough to resemble a unique path, like for the CM in Fig. 7(b) where only two paths can be clearly distinguished. Similarly, at high frequency all the apparent curves tend to compose a unique, well-defined frequency response, both for the CM and the DM, because linear components (functional and parasitic inductors and capacitors) become dominant in circuit dynamics over nonlinear effects.

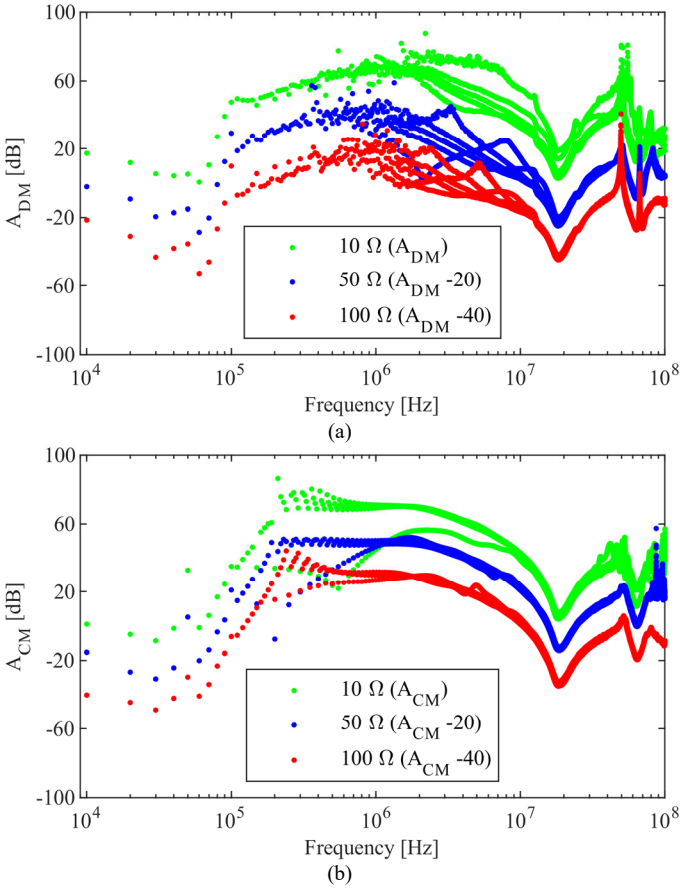

Fig. 9 – (a) DM and (b) CM insertion attenuation of the EMI filter in the step-down converter circuit, for duty cycle δ=0.8 and load R_1=10 Ω (green dots), R_1=50 Ω (blue), R_1=100 Ω (red). To allow readability in a single plot, curves are translated by 0, -20 and -40 dB, respectively.

C. *Impact of Duty Cycle and Load*

It is interesting to confirm the dependence on the harmonic index by modifying the duty cycle, which changes the harmonic sets according to (5). Furthermore, the impact of dc loading conditions is explored here.

Fig. 9 reports the CM/DM insertion attenuation for the same duty-cycle δ=0.8 (load voltage 160 V) and for resistors R_1=100 Ω, R_1 = 50 Ω, R_1 = 10 Ω (in different colors). As in Fig. 7, there are up to five apparent curves of attenuation for each loading case.

Fig. 10 reports results for δ=0.75=3/4 (load voltage 150 V) and the three resistors defined above. Accordingly, the period of (5) is n=4 and there are up to four apparent curves of attenuation resulting from the accumulation of dots. Finally, Fig. 11 shows results for δ=0.5=1/2 (load voltage 100 V) and the three load resistors. In this case, the period of (5) is n=2 therefore there are up to two apparent curves of attenuation.

In all the plots, the dependence on loading conditions is strong below 10 MHz, with greater impact on DM than on CM.

IV. Impact of Duty-Cycle Instability

Modern crystal oscillators guarantee stability in the order of a few parts per million, therefore variations of the switching frequency are of little practical interest. Conversely, the duty

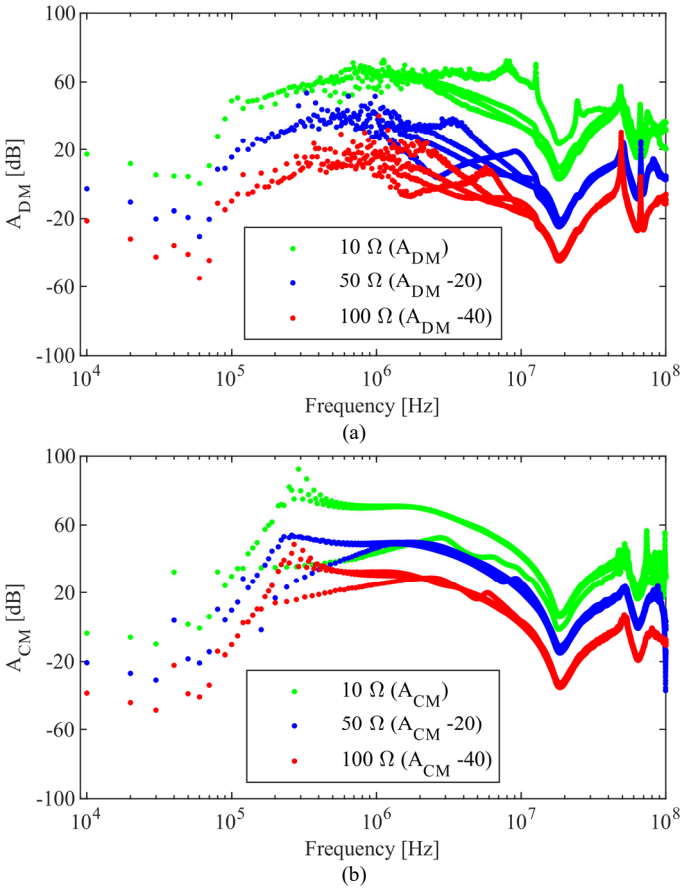

Fig. 10 – (a) DM and (b) CM insertion attenuation of the EMI filter in the step-down converter circuit, for duty cycle δ=0.75 and load R_1=10 Ω (green dots), R_1=50 Ω (blue), R_1=100 Ω (red). To allow readability in a single plot, curves are translated by 0, -20 and -40 dB, respectively.

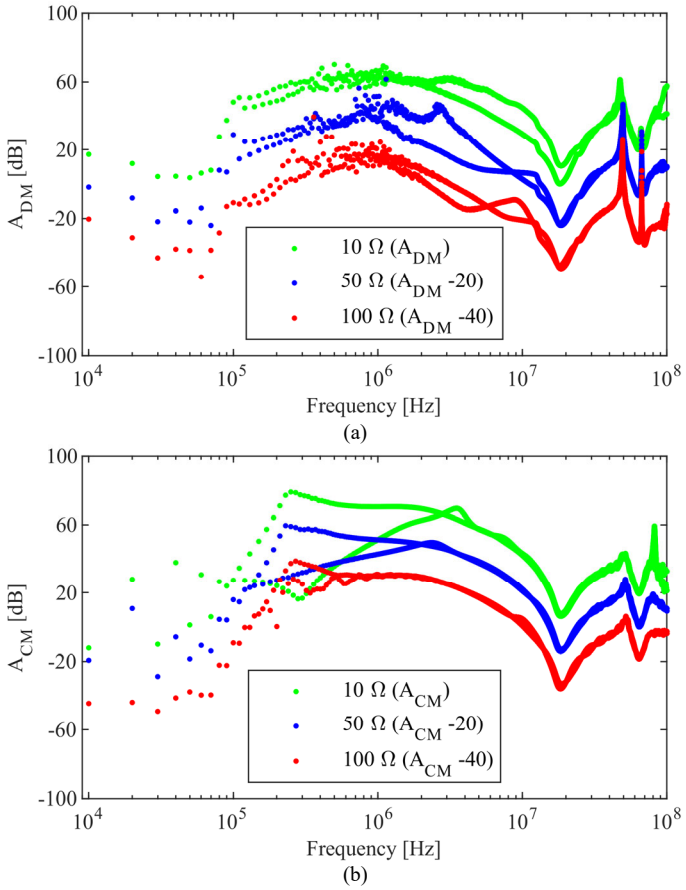

Fig. 11 – (a) DM and (b) CM insertion attenuation of the EMI filter in the step-down converter circuit, for duty cycle δ=0.5 and load R_1=10 Ω (green dots), R_1=50 Ω (blue), R_1=100 Ω (red). To allow readability in a single plot, curves are translated by 0, -20 and -40 dB, respectively.

cycle is normally subject to random deviations since it is synthesized by control circuitries implementing comparators and feedback controllers. Since previous simulations are founded over strong properties related to the existence of specific sets determined by the duty cycle δ, one may question whether the introduction of randomness may significantly change the outcomes.

SPICE simulations of the circuit in Fig. 5 are reconsidered in this Section by defining the waveform of the driving voltage source V_2 as a train of rectangular pulses with constant period and slightly variable duty cycle. Specifically, the duty cycles of subsequent pulses are independent and uniformly distributed random variables, centered around the average δ and ranging in the interval $[\delta(1-\varepsilon), \delta(1+\varepsilon)]$. Two variational ranges ε=0.05%, 0.5% are investigated with δ=0.8.

Since CE waveforms are no more stationary and periodic, the evaluation of spectra and the definition of harmonic peaks is not univocal and obvious. It is of paramount importance including an algorithm to emulate the operation of an EMI receiver with CISPR RBW, namely, RBW=200 Hz for frequencies between 9 kHz and 150 kHz, and RBW=9 kHz for frequencies between 150 kHz and 30 MHz [8]. This specific choice makes the predicted spectra univocally consistent with standard CE measurements. (Needless to mention, RBW emulation would have been inconsequential in previous Sec. III for a periodic signal with RBW<f_0). Spectra accounting for RBW emulation can then be sampled at the nominal multiple frequencies nf_0 for evaluating the insertion attenuation (3). In passing, it is worth mentioning weighting detectors (quasi-peak, peak) as another peculiarity of CISPR measurements. However, they are not implemented in simulation processing since their time constants are large and inconsequential to the investigated phenomenon.

The DM and CM CE for R_1 = 50 Ω are shown in Fig. 12 (ε=0.05%) and in Fig. 13 (ε=0.5%), each plot presenting the spectrum with and without RBW emulation and EMI filter. Without RBW, only low-frequency peaks are individually resolved at each harmonic frequency, whereas spectral lines are spread over the whole frequency range above a few hundreds of kHz (though this could be visually appreciated only by zooming in). RBW emulation retains the resolution of low-frequency peaks and smooth out the high frequency spectrum till a broadband envelope is obtained in the MHz range. Additionally, spectra with RBW emulation prove to be scarcely sensitive to different numerical sets of random duty cycles generated in the simulations (provided they have the same statistical distribution). A greater variation range ε of the duty cycle accentuates the broadband characteristic of CE, as apparent from the comparison between Fig. 12 and 13.

By sampling CE spectra with RBW emulation, insertion attenuations result as in Fig. 14 for ε=0.05% and in Fig. 15 for

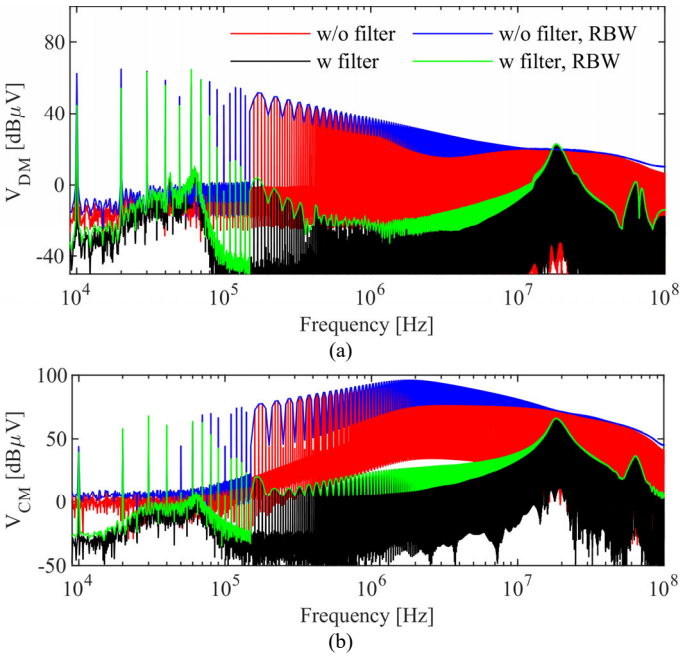

Fig. 12 – (a) DM and (b) CM CE of the step-down converter: without EMI filter (no RBW: red line; with RBW: blue line) and with EMI filter (no RBW emulation: black line; with RBW: green line), for random duty cycle (δ=0.8, ε=0.05%) and load R_l=50 Ω.

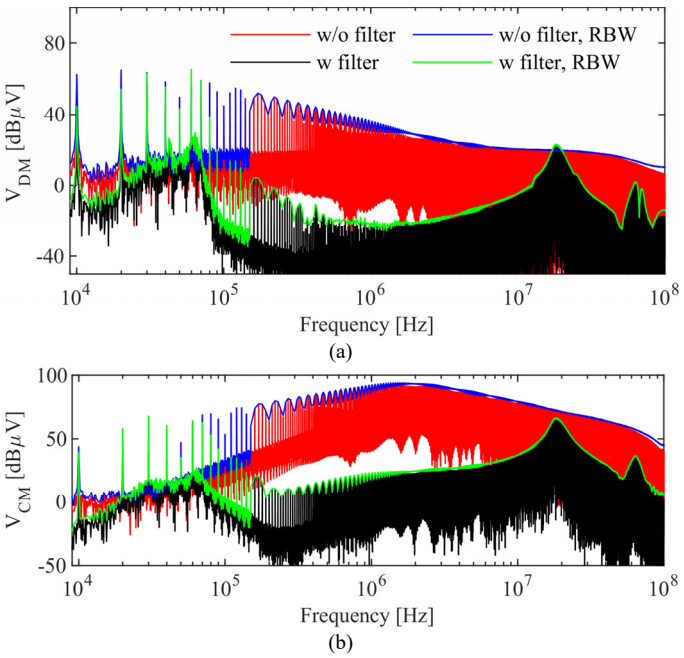

Fig. 13 – (a) DM and (b) CM CE of the step-down converter: without EMI filter (no RBW: red line; with RBW: blue line) and with EMI filter (no RBW: black line; with RBW: green line), for random duty cycle (δ=0.8, ε=0.5%) and load R_l=50 Ω.

ε=0.5%. Results are reported for different loads: R_l = 50 Ω (CE spectra in Fig. 12-13), R_l = 100 Ω and R_l = 10 Ω. These plots directly compare to previous Fig. 9. It appears that the dependence on sets of harmonic indexes is greatly mitigated by duty-cycle randomness. Namely, the previous (up to five) apparent curves of attenuation in Fig. 9 tend to bound together, remaining partially recognizable in Fig. 14, whereas they practically merge into a thick line in Fig. 15. Hence, for large duty-cycle instability, the insertion attenuation resembles a

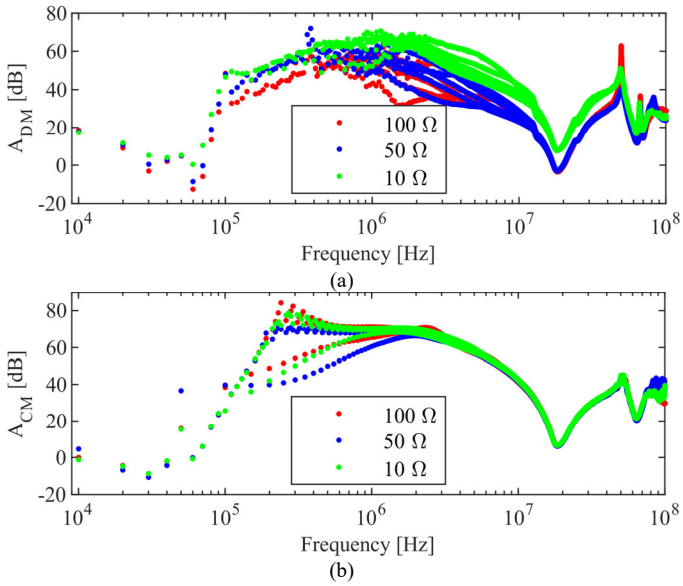

Fig. 14 – (a) DM and (b) CM insertion attenuation of the EMI filter in the step-down converter circuit, for random duty cycle (δ=0.8 ε=0.05%) and load R_l=100 Ω (red dots), R_l=50 Ω (blue), R_l=10 Ω (green).

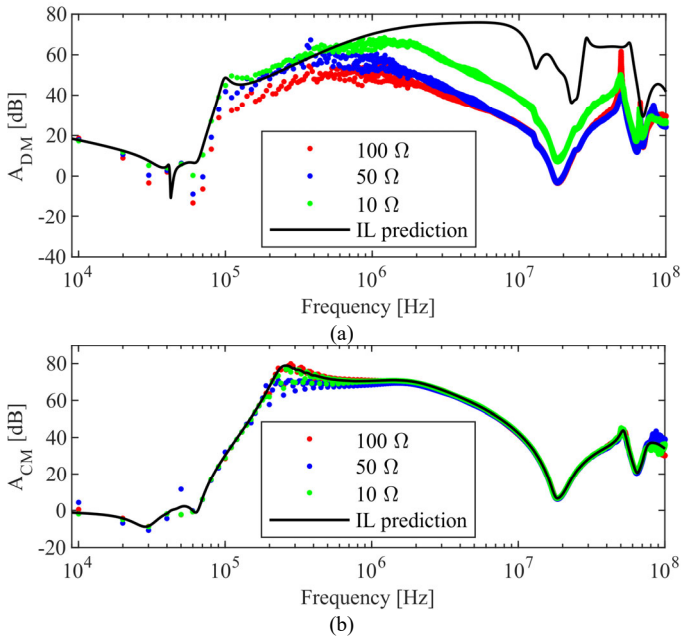

Fig. 15 – (a) DM and (b) CM insertion attenuation of the EMI filter in the step-down converter circuit, for random duty cycle (δ=0.8 ε=0.5%) and load R_l=100 Ω (red dots), R_l=50 Ω (blue), R_l=10 Ω (green). Solid black lines are IL frequency responses described in Sec. V.

well-defined frequency response which shows significant dependence on loading conditions only for the DM.

V. Limitation of Linear IL Prediction Models

It is worth investigating whether the well-established concept of IL of linear circuits may be extended to provide reasonable prediction of filter attenuation in a nonlinear switching circuit. This question arises in view of the tendency to a well-defined frequency response of CM and DM attenuations observed in the previous section for significant duty-cycle random variations. Additionally, as mentioned in Sec. I, several CE modeling approaches presented in the literature [1]-[4] are based on the

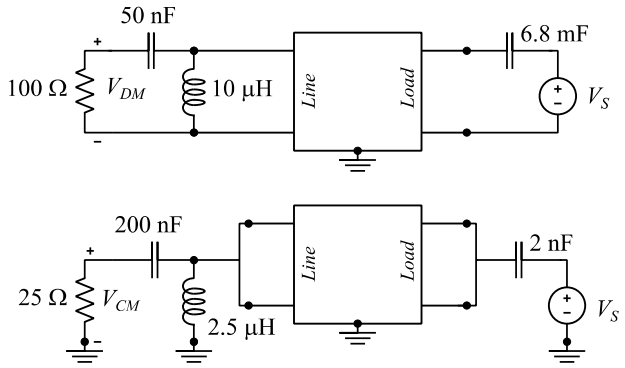

Fig. 16 – Linear circuits for frequency-domain simulations of the IL, involving the dominant terminal impedances of the step-down converter circuit in Fig. 5 in place of the standard resistors in Fig. 1: Symmetrical mode (DM); Bottom: Asymmetrical mode (CM).

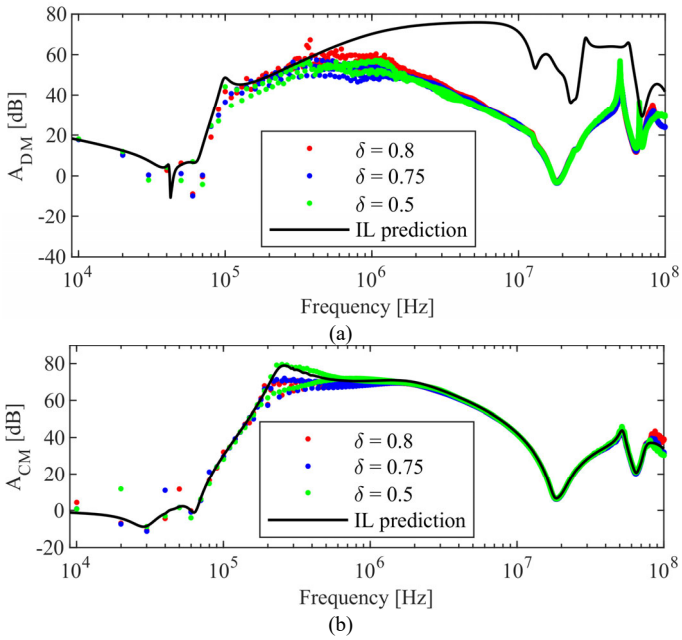

Fig. 17 – (a) DM and (b) CM insertion attenuation of the EMI filter in the step-down converter circuit for load R_1=50 Ω, random duty cycle (ε=0.5%) with different average δ=0.8 (red dots), δ=0.75 (blue), δ=0.5 (green). Solid black lines are IL frequency responses described in Sec. V.

extraction (by measurement or simulation) of linear active and/or passive behavioral models of power-electronic equipment, suggesting that at, the frequency of interest for CE analysis, the behavior of those systems can be reasonably predicted in the frequency domain.

To investigate this aspect, circuits presented in Fig. 16 are intended to replace those presented in Fig. 1, by substituting the standard source and load resistors R_S, R_L with dominant modal impedances easily inferred by inspecting Fig. 5. The DM source impedance is dominated by capacitor C_1, whereas the CM source impedance is dominated by the parallel of C_7 and C_8. Similarly, the DM and CM load impedances are dominated by the CISPR-25 LISN circuit elements L_2, L_3, C_5, C_6, R_4, R_5.

The frequency response of modal ILs can be evaluated as in (1)-(2) by fast SPICE frequency-domain simulations involving such terminal impedances (with and without EMI filter). Results are added with solid black lines in previous Fig. 15 to

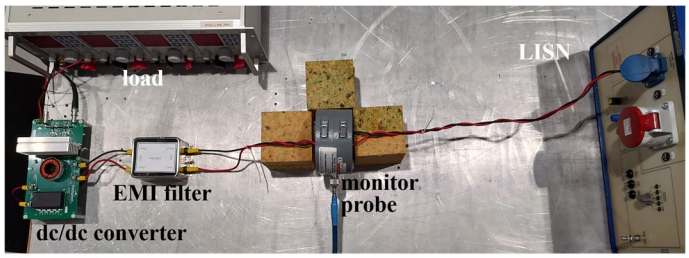

Fig. 18 - Test setup to assess properties of the insertion attenuation of an EMI-filter for a dc/dc converter.

compare with the insertion attenuation in different loading conditions. Additionally, results are plotted in Fig. 17 to compare with the insertion attenuation for different average duty cycles δ=0.8, 0.75, 0.5, ε=0.5%, R_1 = 50 Ω.

It appears that CM attenuation is estimated very well by the linear CM IL, except for limited frequency intervals where results are sensitive to load and duty cycle. Conversely, the DM attenuation of the nonlinear switching circuit is not reasonably predicted by the frequency response of the linear IL (actually, it is largely overestimated). Furthermore, the dependence of DM attenuation with loading conditions and average duty cycle is significant and cannot be inferred from a linear IL circuit model.

VI. Experimental Evidence

This section provides experimental support to corroborate the existence and relevance of the phenomena unveiled by circuit simulation in Sections III-IV. Accordingly, modeling of specific power-electronic equipment and the comparison of measured and predicted CE spectra are out of interest, while the focus is on the EMI filter and whether its attenuation exhibits the peculiar behavior previously observed. In line with this aim, the test setup involves a different buck converter (a commercial device whose functional and parasitic parameters are mostly unknown), whereas the EMI filter is the same considered for exemplification in previous sections.

The main elements of the test setup are pictured in Fig. 18, namely, an electronic load (setting 16 Ω resistance), the dc/dc converter (switching frequency f_0=10 kHz), the EMI filter, the LISN (fed by a 30 Vdc source not shown), and a metallic ground plane. Since the available LISN has only one selectable output channel, modal voltage measurement is not possible, therefore a monitor probe is used to sense the CM/DM current. Measurements are carried out by a Keysight N9038A EMI Receiver, with quasi-peak detector and fast time-domain scan. At each harmonic of f_0, modal filter attenuation is evaluated in logarithmic units by the difference

$$A_X^{(\mathrm{dB})} = I_{X,WO}^{(\mathrm{dB\mu A})} - I_X^{(\mathrm{dB\mu A})} \tag{6}$$

where X=*DM* or X=*CM*, $I_{X,WO}^{(\mathrm{dB}\mu\mathrm{A})}$ is the modal current measured without the EMI filter, and $I_X^{(\mathrm{dB}\mu\mathrm{A})}$ is the modal current measured with the EMI filter.

To explore the dependance of A_X with the harmonic index, narrow RBWs were set on the receiver (100 Hz in the range 9-150 kHz, 1 kHz in the range 0.15-100 MHz). Results are

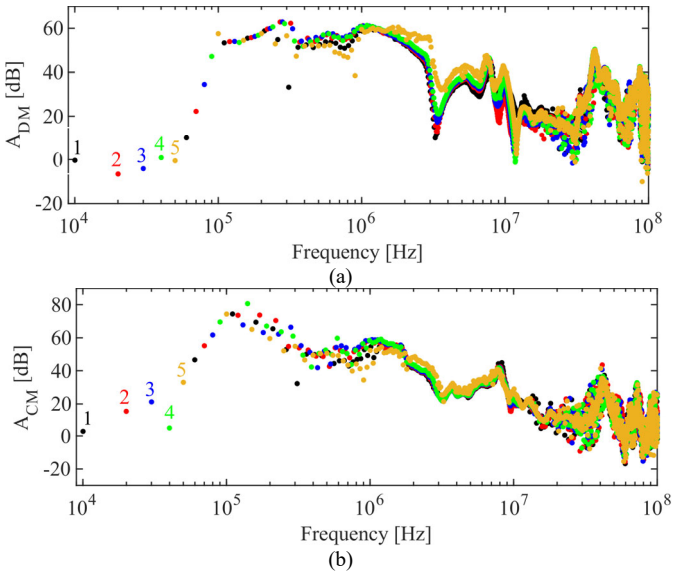

Fig. 19 – (a) Measured DM and (b) CM insertion attenuation for duty cycle δ=0.8 (five sets of harmonic indexes highlighted by different colors).

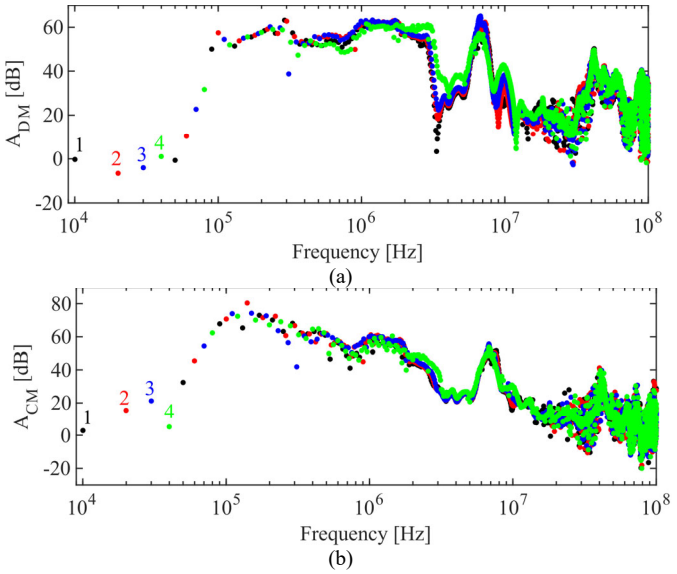

Fig. 20 – (a) Measured DM and (b) CM insertion attenuation for duty cycle δ=0.75 (four sets of harmonic indexes highlighted by different colors).

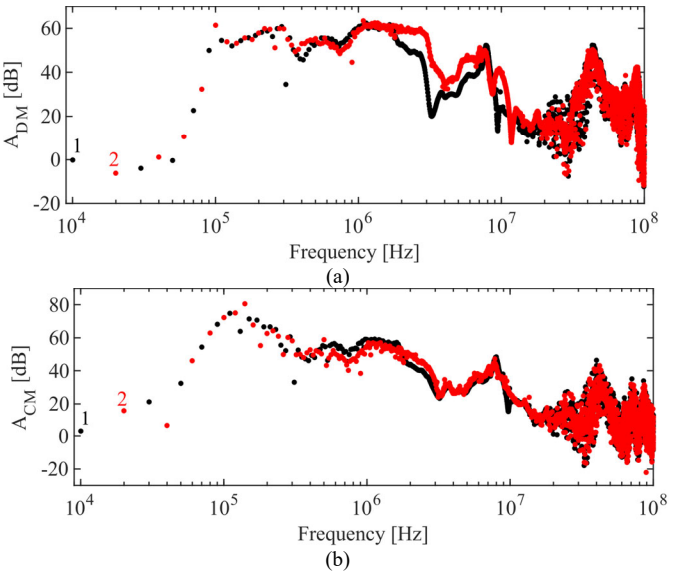

Fig. 21 – (a) Measured DM and (b) CM insertion attenuation for duty cycle δ=0.5 (two sets of harmonic indexes highlighted by different colors). The RBW is 100 Hz in 9-150 kHz and 1 kHz in 0.15-100 MHz.

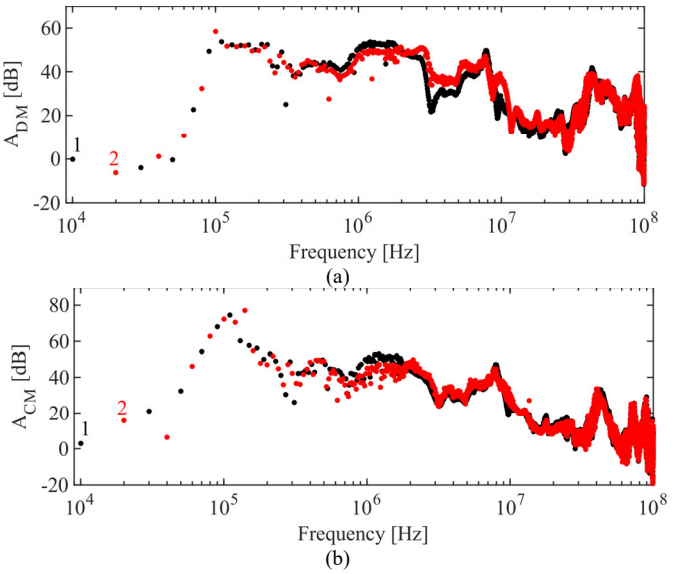

Fig. 22 – (a) Measured DM and (b) CM insertion attenuation for duty cycle δ=0.5 as in Fig. 21 but with broader RBWs (CISPR 200 Hz in 9-150 kHz, 9 kHz in 0.15-100 MHz). The two apparent lines of dots get closer and less chaotic, with tendency towards a well-defined frequency response.

reported in Fig. 19, Fig. 20 and Fig. 21 for duty cycles δ=0.8, δ=0.75 and δ=0.5, respectively.

These plots confirm the existence of apparent lines resulting from the accumulation of dots for each set of harmonic indexes that can be theoretically related to the duty cycle by (5), namely, five, four and two sets, respectively (see Sec. III.B). As observed by simulations, the apparent lines are clearly separated at low frequency (indicatively below 10 MHz), whereas they tend to merge at high frequency.

Furthermore, as these plots are obtained by measurement of real equipment, they include phenomena discussed in Section IV related to random duty-cycle instability. Specifically, one should observe the convergence of apparent lines towards a unique well-defined frequency response with increasing RBW. To exemplify this property, measurements for the case δ=0.5 are newly reported in Fig. 22 as obtained by setting broader RBWs (the standard CISPR 200 Hz and 9 kHz). By comparing Fig. 21 and Fig. 22 the convergence is clearly visible, with a more remarkable effect for DM as expected.

VII. Conclusion

In this paper, time-domain circuit simulation was proposed to characterize the suppression characteristics of filters in nonlinear power-electronic circuits. Circuit simulation requires a component-level representation of the converter, and equivalent circuits of the LISN, the EMI filter, and any other component of the system [5]-[14]. CE are computed in time-domain and subsequently transformed into frequency domain by FFT. The advantage of time-domain simulation resides in the representation of valves (diodes, transistors) as nonlinear

elements, which would not be possible in frequency-domain models [1]-[4]. The comparison of CE spectra in the presence and in the absence of the EMI filter allows defining a CM/DM insertion attenuation for each harmonic component, which extends the concept of IL.

For exemplification, the SPICE model of a step-down dc/dc converter was analyzed together with a black-box equivalent circuit of the EMI filter [12]. It was shown that the insertion attenuation behaves quite differently from the standard IL defined in linear setups. The discrete attenuation points do not follow a unique well-defined frequency response. In particular, the duty cycle of the converter determines a number of harmonic sets, each one characterized by its own specific trend in the attenuation plot versus frequency, especially for the lowest portion of the spectrum. Above some MHz, such differences tend to disappear since circuit dynamic becomes dominated by linear components (capacitors, inductors) rather than by the nonlinear characteristics of switching valves. By taking into account the slight random instability of the duty cycle, always present in practice, together with the RBW of the EMI receiver, differences between harmonic sets appear to be mitigated but still present. A test setup involving a buck converter provided experimental support to corroborate the existence and relevance of the phenomena unveiled by circuit simulation. It is worth stressing that the discussed properties are limited to the category of dc/dc converters, that is, converters whose switching is characterized by a fixed duty cycle. Conversely, the spectrum of CE in dc/ac converters is determined by pulse-width modulation and is not simply composed of harmonics of the switching frequency, therefore further ad hoc investigations are required.

Linear setups for the definition of the CM/DM IL can be improved by accounting for the dominant high-frequency CM/DM impedances at the line and load side of the filter instead of standard resistors, but their outcome exhibits reasonable accuracy for the CM attenuation only, which is scarcely dependent on the duty cycle and the load. Conversely, this approach does not lead to satisfactory predictions for DM attenuation, which shows dependence on those functional parameters. Only time-domain circuit simulations can properly model the low-frequency functional operation of the converter together with the high-frequency EMI emission spectrum. Overall, the proposed insertion attenuation and its properties, either observable by numerical prediction or experimental measurement, put in evidence some limits of the classic IL concept which may be addressed by new research objectives in standardization [15].

REFERENCES

[1] Q. Liu, F. Wang, and D. Boroyevich, "Modular-Terminal-Behavioral (MTB) model for characterizing switching module conducted EMI generation in converter systems," *IEEE Trans. Power Electronics*, vol. 21, no. 6, pp. 1804-1814, Nov. 2006.

[2] A. Perez, A. M. Sanchez, J. R. Regue, M. Ribo, P. Rodriguez-Cepeda, F. J. Pajares, "Characterization of power-line filters and electronic equipment for prediction of conducted emissions," *IEEE Trans. Electromagn. Compat.*, vol. 50, no. 3, pp. 77-585, Aug. 2008.

[3] H. M. Rebholz, S. Tenbohlen, and W. Kohler, "Time-domain characterization of rf sources for the design of noise suppression filters," *IEEE Trans. Electromagn. Compat.*, vol. 51, no. 4, pp. 945-952, Nov. 2009.

[4] G. Spadacini, F. Grassi, D. Bellan, S. A. Pignari, and F. Marliani, "Prediction of conducted emissions in satellite power buses," *Int. Journal Aerospace Engineering*, vol. 2015, pp. 1-10, 2015.

[5] E. Rondon, F. Morel, C. Vollaire, and J.-L. Schanen, "Modeling of a buck converter with a SiC JFET to predict EMC conducted emissions," *IEEE Trans. Pow. Electr.*, vol. 29, no. 5, pp 2246-2260, May 2014.

[6] G. Spadacini, F. Grassi, and S. A. Pignari, "Modelling and simulation of conducted emissions in the powertrain of electric vehicles," *Progress in Electromagn. Res. B*, vol. 69, page 1-15, 2016.

[7] Y. Liu, K. Y. See, S. Yin, R. Simanjorang, A. K. Gupta, and J. Lai, "Equivalent circuit model of high-power density SiC converter for common-mode conducted emission prediction and analysis," *IEEE Electromagn. Compat. Mag.*, vol. 8, no. 1, pp. 67-74, 2019.

[8] L. Yang, S. Wang, H. Zhao, and Y. Zhi, "Prediction and analysis of EMI spectrum based on the operating principle of EMC spectrum analyzers," *IEEE Trans. Power Electronics*, vol. 35, no. 1, pp. 263–275, 2020.

[9] M. Laour, R. Tahmi, and C. Vollaire, "Modeling and analysis of conducted and radiated emissions due to common mode current of a Buck Converter," *IEEE Trans. Electromagn. Compat.*, vol. 59, no. 4, pp. 1260-1267, Aug. 2017.

[10] S. Wang, F. C. Lee, and W. G. Odendaal, "Characterization and parasitic extraction of EMI filters using scattering parameters," *IEEE Trans. Power Electronics*, vol. 20, no. 2, pp. 502–510, 2005.

[11] C. Dominguez-Palacios, P. Gonzalez-Vizuete, M. A. Martin-Prats, and J. Bernal-Mendez, "Smart shielding techniques for common mode chokes in EMI filters," *IEEE Trans. Electromagn. Compat.*, vol. 61, no. 4, pp. 1329–1336, Aug. 2019.

[12] S. Negri, G. Spadacini, F. Grassi, and S. A. Pignari, "Black-box modeling of EMI filters for frequency and time-domain simulations," *IEEE Trans. Electromagn. Compat.*, early access, 2021.

[13] I. Stevanovic, S. Skibin, M. Masti, and M. Laitinen, "Behavioral modeling of chokes for EMI simulations in power electronics," *IEEE Trans. Power Electronics*, vol. 28, no. 2, pp. 695-705, Feb. 2013.

[14] H. Zhao, D. Dalal, J. K. Jørgensen, M. M. Bech, X. Wang, and S. Munk-Nielsen, "Behavioral modeling and analysis of ground current in medium-voltage inductors," *IEEE Trans. Power Electronics*, vol. 36, no. 2, pp. 1236 – 1241, Feb. 2021.

[15] CISPR 17, *Methods of measurement of the suppression characteristics of passive EMC filtering devices*, IEC, Jun. 2011.

[16] L. O. Chua, C. A. Desoer, E. S. Kuh, *Linear and Nonlinear Circuits*, McGraw-Hill, 1987.

[17] Linear Technology Inc., *LTspice IV Getting Started Guide*, 2011. Available at: https://www.analog.com/en/design-center/design-tools-and-calculators/ltspice-simulator.html

[18] S. Negri, G. Spadacini, F. Grassi, S. A. Pignari, October 27, 2021, "EMI-Filter Black-Box SPICE Model", IEEE Dataport, doi: https://dx.doi.org/10.21227/ydw2-sm33

[19] CISPR 25, *Vehicles, boats and internal combustion engines - Radio disturbance characteristics - Limits and methods of measurement for the protection of on-board receivers*, IEC, Oct. 2016.